AMERICAN JOURNAL OF PHYSIOLOGY
GASTROINTESTINAL AND LIVER PHYSIOLOGY

Am J Physiol Gastrointest Liver Physiol 326: G3–G15, 2024.
First published October 24, 2023; doi:10.1152/ajpgi.00297.2022

RESEARCH ARTICLE

Inter-Organ Communication in Homeostasis and Disease

Respiratory exposure to agricultural dust extract promotes increased intestinal *Tnfα* expression, gut barrier dysfunction, and endotoxemia in mice

Meli'sa S. Crawford,[1] Arzu Ulu,[1] Briana M. Ramirez,[2] Alina N. Santos,[1] Pritha Chatterjee,[1] Vinicius Canale,[1] Salomon Manz,[1] Hillmin Lei,[1] Tara M. Nordgren,[1,3] and Declan F. McCole[1]

[1]*School of Medicine, Division of Biomedical Sciences, University of California, Riverside, California, United States;*
[2]*Department of Biochemistry and Molecular Biology, University of California, Riverside, California, United States; and*
[3]*Department of Environmental and Radiological Health Sciences, Colorado State University, Fort Collins, Colorado, United States*

Abstract

Concentrated animal feeding operations (CAFOs) are responsible for the production of global greenhouse gases and harmful environmental pollutants including hydrogen sulfide, ammonia, and particulate matter. Swine farmers are frequently exposed to organic dust that is proinflammatory in the lung and are thus at greater risk of developing pneumonia, asthma, and other respiratory conditions. In addition to respiratory disease, air pollutants are directly associated with altered gastrointestinal (GI) physiology and the development of GI diseases, thereby highlighting the gut-lung axis in disease progression. Instillation of hog dust extract (HDE) for 3 wk has been reported to promote the development of chronic airway inflammation in mice, however, the impact of HDE exposure on intestinal homeostasis is poorly understood. We report that 3-wk intranasal exposure of HDE is associated with increased intestinal macromolecule permeability and elevated serum endotoxin concentrations in C57BL/6J mice. In vivo studies also indicated mislocalization of the epithelial cell adhesion protein, E-cadherin, in the colon as well as an increase in the proinflammatory cytokine, *Tnfα*, in the proximal colon. Moreover, mRNA expression of the Paneth cell-associated marker, *Lyz1*, was increased the proximal colon, whereas the expression of the goblet cell marker, *Muc2*, was unchanged in the epithelial cells of the ileum, cecum, and distal colon. These results demonstrate that airway exposure to CAFOs dusts promote airway inflammation and modify the gastrointestinal tract to increase intestinal permeability, induce systemic endotoxemia, and promote intestinal inflammation. Therefore, this study identifies complex physiological consequences of chronic exposure to organic dusts derived from CAFOs on the gut-lung axis.

NEW & NOTEWORTHY Agricultural workers have a higher prevalence of occupational respiratory symptoms and are at greater risk of developing respiratory diseases. However, gastrointestinal complications have also been reported, yet the intestinal pathophysiology is understudied. This work is novel because it emphasizes the role of an inhaled environmental pollutant on the development of intestinal pathophysiological outcomes. This work will provide foundation for other studies evaluating how agricultural dusts disrupts host physiology and promotes debilitating gastrointestinal and systemic disorders.

agricultural pollution; gut-lung axis; intestinal barrier function; LPS

INTRODUCTION

Concentrated animal feeding operations (CAFOs) are a major contributor to air pollution, reduced air quality, and increased mortality in the United States (1). Recent studies suggest more than 17,900 deaths have been instigated by the inhalation of emissions produced from livestock waste and dusts containing particulate matter (PM, e.g., NH_3), fungi, bacteria, and bacterial byproducts (1, 2). More specifically, agricultural work is associated with occupational respiratory disorders (e.g., chronic obstructive pulmonary disease and asthma) and nonpulmonary diseases (e.g., cancer and cardiovascular disease) seemingly from prolonged exposure to CAFO dust (3–6). Indeed, studies have identified the pathophysiological consequences of prolonged agricultural dust and PM exposure on the development of chronic airway inflammation in animal models (7–10). However, studies also suggest that environmental pollution and particulate matter inhalation can promote adverse effects in the gastrointestinal tract (11, 12), thereby highlighting the potential for communication between the lungs and the gastrointestinal tract (gut-lung axis). Inhaled particulates deposited in the

Correspondence: D. F. McCole (declan.mccole@ucr.edu).
Submitted 3 January 2023 / Revised 18 October 2023 / Accepted 19 October 2023

nasopharyngeal compartment and airways can be removed via mucociliary clearance, swallowed, and further cleared via the gastrointestinal tract (5, 12). An epidemiological study found that nonspecific abdominal pain was associated with short-term exposure to air pollution among young adults (5). In addition, in vivo work demonstrated that male Swiss albino mice exhibited abdominal pain following acute gavage of urban particulates and a delay in colonic transit following chronic exposure (5). Moreover, following acute gavage of urban particulate matter (200 μg/mL), male C57BL/6 mice displayed intestinal epithelial cell death, inflammation, and increased intestinal permeability (11). Furthermore, environmental particulate matter exposure has been reported to increase proinflammatory cytokine secretion, intestinal permeability, and alter short-chain fatty acid and microbial composition in interleukin (IL)-10$^{-/-}$ mice (12). Interestingly, farmers and farmworkers used in swine confinement facilities exhibit a higher prevalence of airway diseases including chronic bronchitis (8) and acute symptoms such as headache, fever, and chest tightness (2) than other animal farmers (e.g., cattle, poultry, and sheep; 13). Furthermore, epidemiological studies have demonstrated that swine confinement facility workers show enhanced decline in lung function (14) and report a variety of symptoms including dyspnea, fever and chills, and nausea (15–17). Prior studies have compared the composition of dusts collected from different CAFO facilities and found that the pathogenicity of swine farm dusts is derived from the presence of endotoxins in combination with higher proportions of gram-positive bacteria and peptidoglycans (2). Moreover, repetitive exposure models demonstrate that intranasally exposing mice to hog dust extract (HDE) for 3 wk results in significant lung inflammatory and pathological responses (8, 9, 18). Given the evidence of chronic airway inflammation following HDE instillation and the impact of inhaled environmental particulate matter on intestinal barrier function, the aim of the current study was to examine the effects of repetitive HDE exposure on intestinal homeostasis and further elucidate the role of the gut-lung axis in intestinal disease manifestations identified in swine farm workers.

METHODS

Preparation of Aqueous Hog Dust Extract

Dust extracts were prepared as previously described (19). Briefly, settled dusts were collected from swine confinement facilities and stored at −20°C. To prepare 100% aqueous hog dust extract, 5 g dust was suspended in 50 mL of Hanks' balanced salt solution for 1 h then filtered and sterilized through a 0.22-mm filter (20). The 100% aqueous dust solution was aliquoted and stored at −20°C until used. For instillation, a 12.5% HDE solution was prepared by diluting 100% HDE in sterile phosphate-buffered saline (PBS).

Animals

Eight-week-old male ($n = 6$; 26.2 ± 1.2 g body mass) and female ($n = 6$; 20.3 ± 1.2 g body mass) C57BL/6J mice were purchased from Jackson Laboratories (Bar Harbor, ME) and were group housed in microisolator cages with free access to food (standard chow) and water. Mice were acclimatized for 1 wk upon arrival before experimentation. Body weight was measured daily, and fecal samples were collected weekly.

Murine Model of Dust Exposure

C57BL/6J mice were intranasally treated with HDE [12.5%, 22.1–91.1 EU (endotoxin unit)/mL; 3 females and 3 males, $n = 6$] or sterile phosphate-buffered saline (PBS; 50 μL; 3 females and 3 males, $n = 6$) control, daily for 3 wk (5 consecutive days/wk) under light sedation (repetitive exposure), as previously described (8). The 12.5% HDE concentration has been shown to promote maximal immune response with negligible toxicity in mice (8, 21). On *day 14*, an HDE-treated male succumbed to treatment complications and was excluded from the study. Remaining study animals were terminally anesthetized with isoflurane (Cat. No. NDC-11695-6776-2, Henry Schein, Melville, NY) on *day 15*. Five hours postexposure, bronchoalveolar lavage fluid (BALF) was collected three times with 1 mL of sterile saline each time. BALF was centrifuged, and pelleted cells were stained and counted with Diff-Quik (Siemens, Newark, DE). All procedures were approved by the University of California, Riverside Institutional Animal Care and Use Committee (McCole 20190032; Nordgren; 20200014).

Quantification of Lung Immune Cell Infiltration

At the end of the 15-day instillations, mice were euthanized, and trachea was cannulated to collect bronchoalveolar lavage fluid (BALF) from each mouse. BALF collection incorporated three separate washes with 1 mL of phosphate-buffered saline (PBS). Washes were centrifuged at 1,200 rpm for 5 min. Pelleted cells from all washes were combined and counted. Cytospin slides were prepared using 100,000 cells and stained with Diff-Quik kit (Siemens, Newark, DE), and differential cell counts were obtained as previously described (9). In addition, lung inflammation was evaluated by quantification of alveolar inflammation (18). Peribronchial regions were evaluated by scanning the entire lung section with ×20 and ×40 objectives and then enumerating the number of cells in the alveolar sacs in a total of five images at ×40 objective, which resulted in five values of each mouse (18). An average of these values represented one mouse in statistical analysis (18).

Examination of Intestinal Permeability In Vivo

To examine the effects of 12.5% HDE exposure on intestinal permeability, study animals were given two probes: 80 mg/mL FITC-dextran (4 kDa; Cat. No. 46944-500MG-F, Sigma-Aldrich, Darmstadt, DE) and 20 mg/mL rhodamine B-dextran (70 kDa; Cat. No. R9379-250M, Sigma-Aldrich, Darmstadt, DE) diluted in ultrapure water. Before the final instillation on *day 15*, mice were fasted overnight with access to water. The next morning, study animals were challenged with the final dose of PBS or HDE and then given 100 μL of 4 kDa FITC-dextran (FD4) and Rhodamine B dextran-70 kDa (RD70) (FD4/RD70) solution via oral gavage into the stomach. Administration of these different-sized probes allows us to discriminate between tight junction-mediated versus unrestricted intestinal permeability (22, 23). Five hours postexposure and gavage, blood from the inferior vena cava was collected using an insulin syringe. Blood samples were

immediately centrifuged, and serum was collected and stored at −80°C until use. Standards were generated from diluted gavage solution, and serum samples were diluted 1:5 in duplicates in a black 96-well plate (Cat. No. 13701, Thermo Fisher Scientific). FD4 and RD70 fluorescence were measured with the Promega GloMax Multi-Detection system (Promega, Madison, WI) at 490 nm excitation/530 nm emission and 555 nm excitation/595 nm emission, respectively.

Tissue Collection

After BALF collection, lungs were inflated with formalin, fixed, and paraffin-embedded for sectioning and staining. The small and large intestines were removed, separated, and placed in PBS. Whole tissue sections of the small intestine (duodenum, jejunum, and ileum) were collected from histology, RNA, and protein analyses. The length of the large intestine (cecum, proximal, and distal colon) was measured. Whole tissue sections were then washed with sterile saline and sectioned for histology, RNA, and protein analyses. To examine morphological changes, intestinal sections were fixed with 10% formalin (Cat. No. HT501128-4L, Sigma-Aldrich, Darmstadt, DE) paraffin-embedded, and sectioned at 5 μm. To isolate intestinal epithelial cells, tissue sections were flushed with PBS and placed in 500 mL of cell recovery solution (Cat. No. CB40253, Corning, Bedford, MA) for 2 h. After a 2-h incubation, tissue sections were shaken and centrifuged at 630 *g* for 10 min (Cat. No. 75002446, Thermo Scientific Sorvall Legend Micro 21 R Centrifuge). Pelleted cells were resuspended and washed with PBS three times. After the final PBS wash, intestinal epithelial cells were aliquoted for future RNA and protein analyses. PBS was aspirated and intestinal epithelial cell aliquots were stored in RLT buffer (Cat. No. 74106, Qiagen, Venlo, NL) or radioimmunoprecipitation assay lysis buffer at −80°C.

Hematoxylin and Eosin, Immunofluorescence, Terminal Deoxynucleotide Transferase dUTP Nick End Labeling, and Periodic Acid Schiff Staining

Paraffin-embedded tissue sections were cut into 5-μm sections, deparaffinized using xylene, and rehydrated in descending alcohol series. For hematoxylin and eosin (H&E), slides were incubated for 1 min in hematoxylin solution (Cat. No. 3530-16, Ricca Chemical Company, Arlington, TX), rinsed in tap water for 30 s, stained with eosin Y solution (Cat. No. HT110132-1L, Sigma-Aldrich, Darmstadt, DE), briefly rinsed in H_2O, dehydrated in ascending alcohol series, and mounted using Permount mounting solution (Cat. No. SP15-500, Fisher Scientific, Hampton, NH). Images were acquired using a Leica microscope model DM5500B coupled with DFC450C camera and LAS AF3.2.0 software for image acquisition (Leica, Nussloch, Germany). Final images were prepared in PowerPoint. Assessment of H&E intestinal sections was conducted at The University of Chicago by a gastrointestinal pathologist. For immunofluorescence, heat-induced antigen retrieval with 10 mM sodium citrate (pH 6.0) was performed for 20 min at 96°C then rinsed with phosphate-buffered saline with Tween (PBST) to remove excess retrieval buffer. Briefly, sections were blocked (2% normal donkey serum, 1% bovine serum albumin, 0.1% Triton-X, 0.05% Tween-20, and 0.05% sodium azide in PBS) for 30 min, incubated with an E-cadherin primary antibody (overnight, 1:800; Cat. No. A748, R&D Systems) and Cy3 secondary antibody (1:1,000; Cat. No. 705-166-147, Jackson ImmunoResearch Laboratories) for 30 min at room temperature. Finally, Prolong Gold with DAPI (Cat. No. P36936) was applied to the slides per the manufacturer's guidelines. Confocal images were acquired on an inverted Zeiss 880. Mean fluorescent intensity (MFI) was calculated for each sample by identifying a region of interest and examining five individual crypts. The mean of each individual crypt was subtracted from the image background, averaged, and used for statistical analyses. Quantification of E-cadherin MFI was done with ImageJ software. To examine the presence of apoptotic cells, following deparaffinization, sections were treated with proteinase k (20 μg/mL; Cat. No. 21627, Millipore Sigma, Darmstadt, DE). Sections were then stained with ApopTag Fluorescein In Situ Apoptosis Detection Kit (Cat. No. S7110; Millipore Sigma, Burlington, MA) per the manufacturer's protocol. A separate set of tissue sections were stained with the Periodic Acid-Schiff (PAS) staining system (Cat. No. 395B, Sigma-Aldrich, Darmstadt, DE) to visualize goblet cells. In the proximal and distal colon, 20 individual crypts were examined from each sample. A ratio was calculated from the nuclei and goblet cell pair then all 20 crypt ratios were averaged and used for statistical analyses. All images were acquired with a Leica microscope model DM5500B coupled with DFC450C camera and LAS AF3.2.0 software (Leica, Nussloch, Germany).

Endotoxin Quantification

Serum and HDE endotoxin concentrations were quantified with a commercially available kit (Cat. No. A39552S, Thermo Fisher Scientific, Rockford, IL) per the manufacturer's protocol.

RNA Extraction, cDNA Synthesis, and qPCR

RNA from intestinal epithelial cells and whole tissue lysates was extracted using the RNeasy Mini Kit (Cat. No. 74106, Qiagen, Venlo, NL), according to manufacturer's protocol. complementary DNA (cDNA) was synthesized from RNA using the qScript cDNA synthesis kit from Quantabio (Cat. No. 95049-500, Beverly, MA) per manufacturer's protocol. iQ SYBR Green Supermix (Bio-Rad, Hercules, CA) was used for real-time quantitative PCR on a C1000 Thermal cycler equipped with a CFX96 real-time PCR system and the Bio-Rad CFX Manager 3.1 Software. The real-time PCR included an initial enzyme activation step (3 min, 95°C) followed by 45 cycles consisting of a denaturing (95°C, 10 s), an annealing (53°–60°C, 10 s), and an extending (72°C, 10 s) step. The PCR included the following steps for each primer: *Il1b* (forward: 5′-TGCCACCTTTTGACAGTGATG-3′ and reverse 5′-GAAGGTCCACGGGAAAGACA-3′), *Tnfα* (forward 5′-ACTCCAGGCGGTGCCTATGT-3′ and reverse 5′-AGTGTGAGGGTCTGGGCCAT-3′), *Il6* (forward 5′-CAACGATGATGCACTTGCAGA-3′ and reverse 5′-TGTGACTCCAGCTTATCTCTTGG-3′), *Il10* (forward 5′-TAGAGCTGCGGACTGCCTTC-3′ and reverse 5′-CTTCACCTGCTCCACTGCCT-3′), *Lyz1* (forward 5′-TGGCTGACTGGGTGTGTTTA-3′ and reverse 5′-TTGATCCCACAGGCATTCTT-3′), *Muc2* (forward 5′-TCCTGACCAAGAGCGAACAC-3′ and reverse 5′-GGGTAGGGTCACCTCCATCT-3′), and *Cdh1* (forward 5′-GCTGGACCGAGAGAGTTACC-3′ and reverse 5′-CCGGGCATTGACCTCATTCT-3′). Measurements were performed in

triplicate and mouse tata box binding protein (Tbp; forward 5′-CACCCCCTTGTACCCTTCAC-3′ and reverse 5′-TGATGACTGCAGCAAATCGC-3′) served as a reference. Data were analyzed by averaging the Ct values and then calculating the ΔCt for each sample. Next, the "Average Ct" values of the control samples were averaged to create a "Control average." Finally, the ΔΔCt and fold gene expression [2^−(ΔΔCt)] values were calculated for each sample.

STATISTICAL ANALYSES

Data were analyzed by paired, unpaired, and Mann–Whitney *U* test. Body weight was analyzed by two-way repeated measures ANOVA with treatment (PBS or HDE) and time (0 or 15 days) as factors. Statistical significance was considered as $P < 0.05$ for all analyses. Data were analyzed using GraphPad Prism 9 software (San Diego, CA).

RESULTS

HDE Exposure Induces Chronic Airway Inflammation

To confirm prior observations with HDE administration, we examined the effects of repetitive HDE exposure on the development of chronic airway inflammation. Lung H&E staining identified immune cell infiltration in alveolar spaces (Fig. 1*A*; $P = 0.018$) and lung tissue (Fig. 1*B*). BALF collected from PBS-treated mice was primarily composed of macrophages (Fig. 2, *A* and *D*), but total BALF macrophages

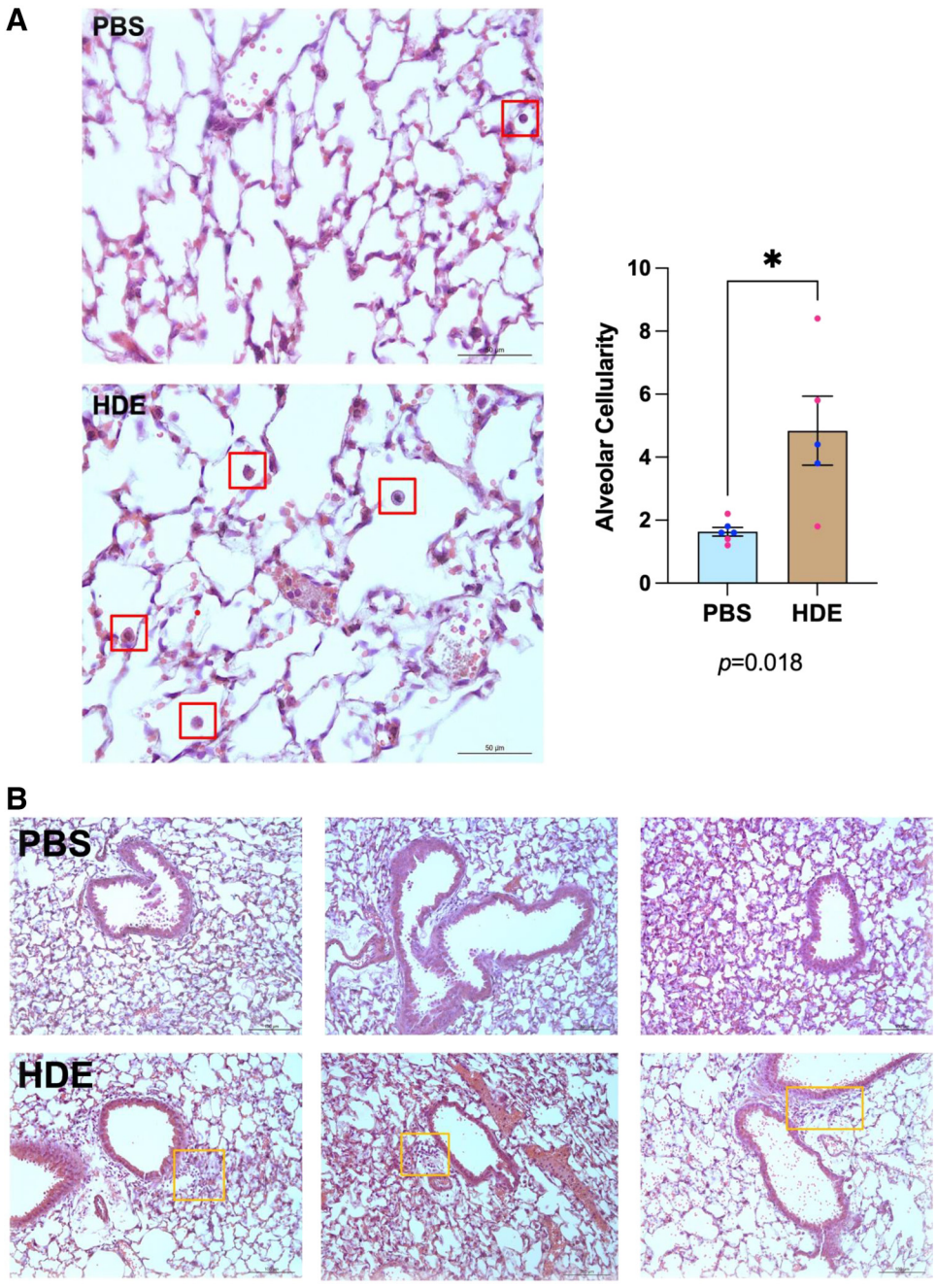

Figure 1. Effects of HDE-treatment on lung morphology. *A*: HDE-treated mice have elevated alveolar cellularity in comparison with saline controls (unpaired *t* test, $*P < 0.05$, $P = 0.018$, $n = 5–6$/group). Red boxes show infiltration of immune cells in alveolar spaces. *B*: H&E-stained paraffin-embedded lung sections of HDE-treated mice show evidence of immune cell infiltration (yellow boxes). The sex of each mouse is depicted by the data point color [light/pink (female) or light/blue (male)]. H&E, hematoxylin and eosin; HDE, hog dust extract.

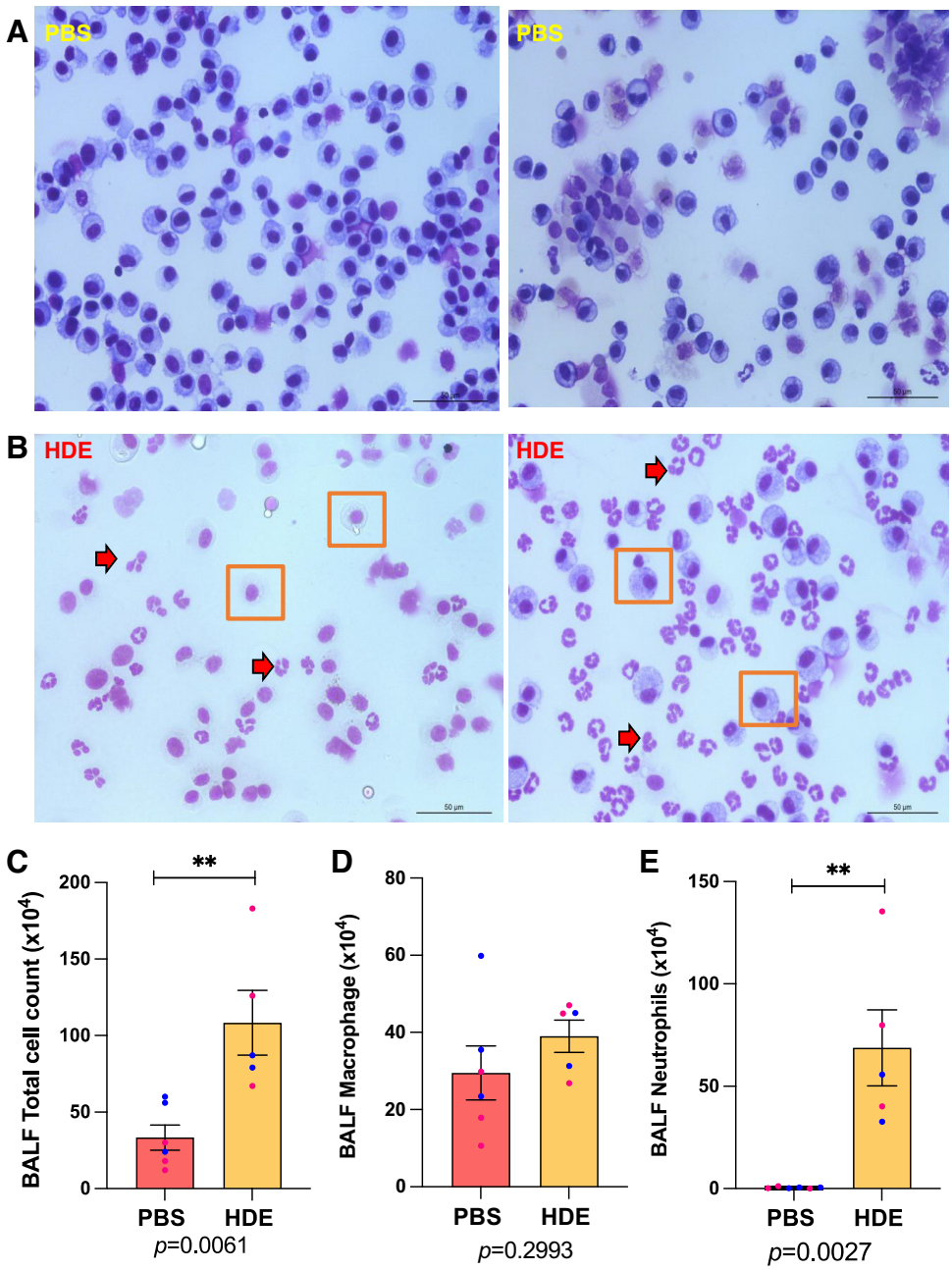

Figure 2. Effects of repetitive HDE exposure on immune cell populations in BALF. *A* and *B*: representative images of BALF collected from PBS- and HDE-treated mice. Orange boxes highlight macrophages found in the BALF whereas the red arrows emphasize neutrophil infiltration. HDE-treated mice exhibited elevated total cell (*C*) and neutrophil levels (*E*) (unpaired *t* test, $^{**}P < 0.01$, $P = 0.0027$ and $P = 0.0061$) in comparison with saline controls. *D*: no changes in macrophage cell count was observed (unpaired *t* test, $P = 0.2993$, $n = 5$–6/group). The sex of each mouse is depicted by the data point color [light/pink (female) or light/blue (male)]. BALF, bronchoalveolar lavage fluid; HDE, hog dust extract; PBS, phosphate-buffered saline.

were not significantly altered (Fig. 2*D*; $P = 0.2993$). However, BALF total cell (Fig. 2*C*; $P = 0.0061$) and neutrophil (Fig. 2*E*; $P = 0.0027$) counts increased significantly following 15-day HDE exposure in comparison with PBS controls. This is consistent with previous reports (8, 9).

Body Weight and Colon Length Were Unaffected by HDE

To further assess the impact of repetitive intranasal HDE exposure in mice, we measured body weight for 15 days and colon length after euthanasia. Previous studies have shown that weight loss and colon shortening are macroscopic indicators of intestinal inflammation in mouse models of colitis (23, 24). Interestingly, repetitive intranasal HDE exposure for 15 days did not significantly alter body weight (Fig. 3*A*; *week 1*, $P = 0.4404$; *week 2*, $P = 0.8685$; *week 3*, $P = 0.9684$), or colon length (Fig. 3*B*; $P = 0.2727$).

Repetitive Intranasal HDE Exposure Increased Intestinal Permeability

Given the development of chronic airway inflammation due to repetitive HDE exposure, we hypothesized that HDE or HDE byproducts may have an indirect effect on intestinal barrier function. To address this hypothesis, we tested how in vivo 4 kDa FITC-dextran (FD4) and rhodamine B dextran 70 kDa (RD70) permeability, markers of tight junction-dependent and independent macromolecule permeability, respectively, were affected following HDE exposure. Repetitive HDE exposure significantly increased FD4 (Fig. 4; $P < 0.0001$) and RD70 (Fig. 4; $P < 0.0001$) permeability in comparison with PBS controls.

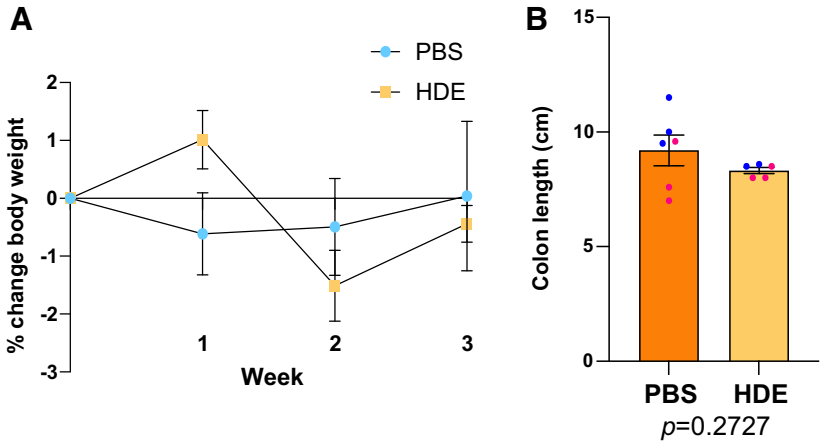

Figure 3. Effects of repetitive HDE exposure on body weight and colon length. *A*: HDE exposure for 15 days did not significantly affect body weight. *B*: no significant differences were seen among the colon lengths of HDE-treated mice (8.32 ± 0.13 cm means ± SE) to that of saline controls (9.2 ± 0.67 cm means ± SE). The sex of each mouse is depicted by the data point color [light/pink (female) or light/blue (male)]. HDE, hog dust extract.

HDE Exposure Induced Serum Endotoxemia

Previous reports have shown that 12.5% HDE has endotoxin levels ranging from 22.9 to 91.1 EU/mL (10). In addition, in vivo models show that physiologically relevant concentrations of bacterial-derived LPS (0.1 mg/kg) can increase intestinal permeability without inducing intestinal mucosal damage (25). In the current study, we found that repetitive HDE-exposure increased levels of serum endotoxins in comparison with saline (Fig. 4*C*; $P < 0.0001$), thereby indicating systemic inflammation.

Alterations in Epithelial Barrier Integrity following HDE Exposure

Although functional data showed evidence of increased FD4 and RD-70 permeability in HDE-treated mice, intestinal morphology remained unchanged as evidenced by H&E staining of the cecum, proximal, and distal colon (Fig. 5). In addition, a terminal deoxynucleotide transferase dUTP nick end labeling (TUNEL) assay was performed to assess the presence of apoptotic cells in the small and large intestine. After HDE-treatment, apoptotic cells were more abundant in the duodenum, jejunum, and ileum (Supplemental Fig. S1, *A*–*C*). However, the presence of TUNEL-positive cells decreased in the distal colon (Supplemental Fig. S1, *D* and *E*; proximal and distal colon). This titration effect may be indicative of a diluted luminal exposure to HDE and HDE-byproducts moving distally down the length of the intestine that predominantly promote apoptosis in the small intestine rather than the colon. To further examine epithelial barrier integrity, IF staining of a key component of adherens junctions, E-cadherin, was performed on intestinal tissue sections. Upon inspection, staining revealed mislocalization and disruption of E-cadherin in the proximal and distal colon of HDE-treated mice (Fig. 6, *A* and *B*). Measurement of E-cadherin fluorescence intensity (MFI) showed a significant decrease in the proximal colon and a decreasing trend in the distal colon of HDE-treated mice (proximal colon, $P = 0.0337$; distal colon, $P = 0.1975$; Fig. 6*C*).

HDE Treatment Increased Ileal Expression of the Proinflammatory Cytokine, Tnfα

To further identify intestinal responses initiated by HDE, inflammatory genes were examined in intestinal whole tissue lysates by qPCR. Interestingly, *Il1b*, *Il6*, and *Il10* mRNA expressions were not significantly different between the ileum or colon of saline and HDE-treated mice ($P > 0.05$, Fig. 7). However, *Tnfα* expression was increased in the proximal colon ($P = 0.0173$) but not in the ileum ($P = 0.1143$), cecum ($P = 0.7875$), and distal colon ($P = 0.6219$) of HDE-treated mice (Fig. 7). Together, these findings suggest that airway exposure to CAFOs dusts promotes airway inflammation and

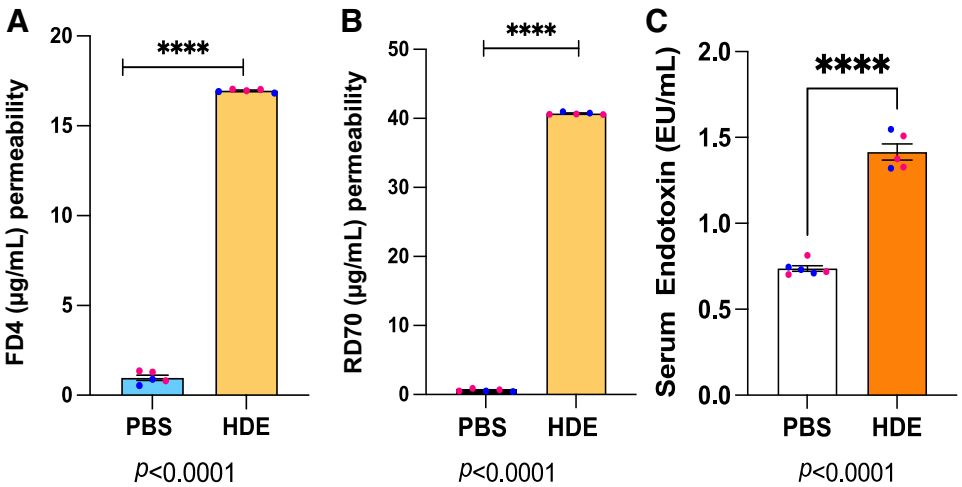

Figure 4. HDE-treatment effects on intestinal permeability. HDE increased permeability to FITC-dextran 4 kDA (*A*) and rhodamine B-dextran 70 kDA (unpaired *t* test, ****$P < 0.001$, $n = 5$–6/group; *B*). *C*: in addition, HDE-treated mice have elevated serum endotoxin levels in comparison with saline controls (unpaired *t* test, ****$P < 0.0001$, $n = 5$–6/group). The sex of each mouse is depicted by the data point color [light/pink (female) or light/blue (male)]. HDE, hog dust extract.

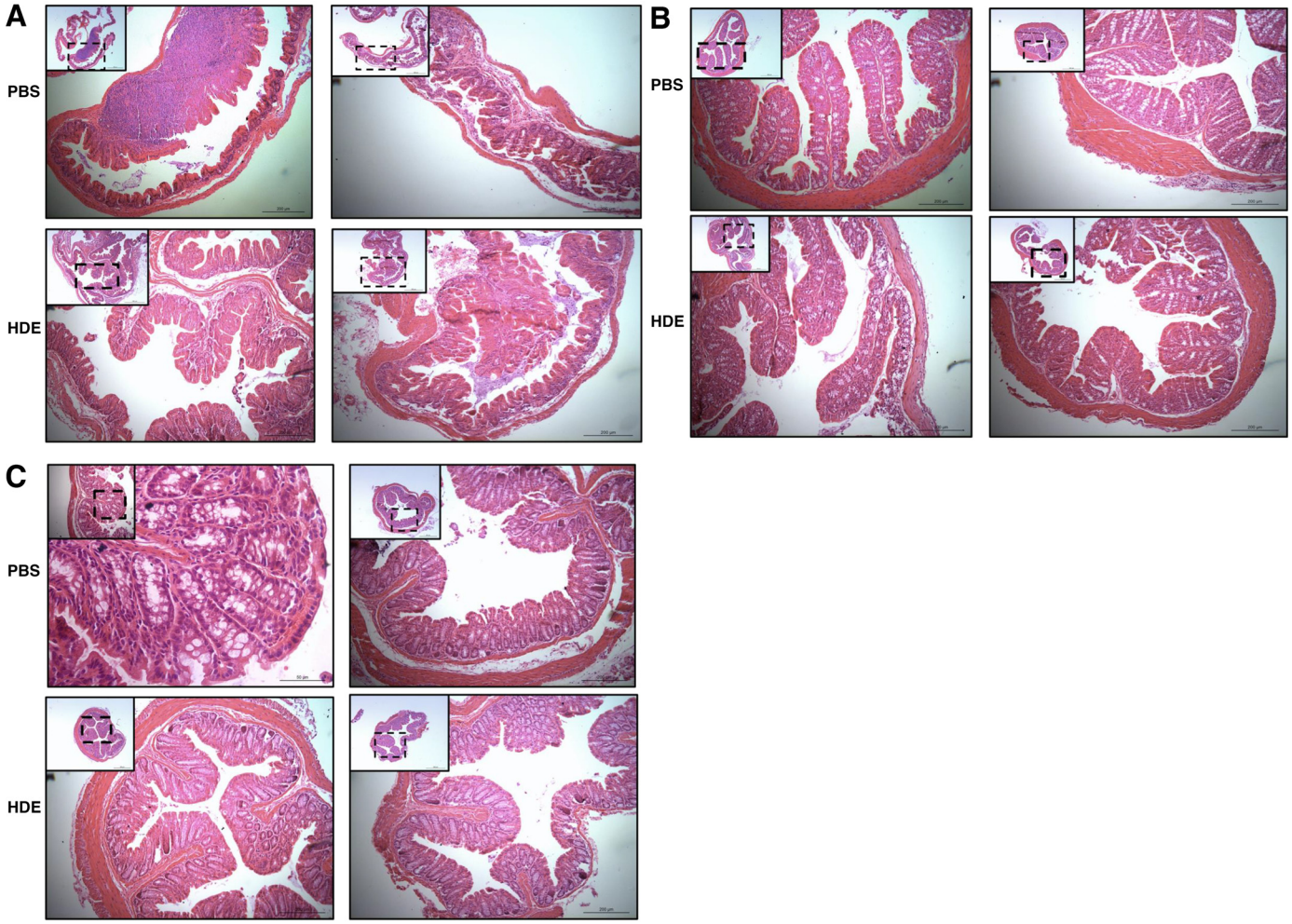

Figure 5. H&E examination of cecum, proximal, and distal colon following repetitive HDE exposure. Representative images show no histological changes observed by hematoxylin and eosin staining in the cecum (*A*), proximal colon (*B*), and distal colon (*C*) of HDE-treated mice ($n = 5$–6/group) in comparison with saline controls ($n = 6$/group). The sex of each mouse is depicted by the data point color [light/pink (female) or light/blue (male)]. H&E, hematoxylin and eosin; HDE, hog dust extract.

can access the gastrointestinal tract to increase regulated and/or unrestricted intestinal permeability.

HDE Treatment Increases Colonic Lyz1 Expression

We next investigated the effects of HDE on other aspects of intestinal barrier defense. After HDE treatment, the Paneth cell-associated antimicrobial marker, *Lyz1* (lysozyme), was increased in proximal colon epithelial cells (Fig. 8, $P = 0.0034$). However, mRNA expression of the goblet cell marker *Muc2* was unchanged in small and large intestinal epithelial cells of HDE-treated mice (ileum, $P = 0.6354$; cecum, $P = 0.2468$; proximal colon, $P = 0.6406$; distal colon, $P = 0.1676$). Moreover, the number of goblet cells measured in the colon was unchanged following HDE treatment (Fig. 9, *A*–*C*, $P < 0.05$).

DISCUSSION

Epidemiological data suggest that airborne pollutants are a major contributor to the development and progression of airway diseases including chronic obstructive pulmonary disease and asthma (26–28). However, animal studies have demonstrated that environmental factors may play a role in modulating the pathogenesis of gastrointestinal disorders (i.e., appendicitis; 5, 29). Based on past observations showing altered gut physiology from exposure to environmental pollutants (2, 12), the goal of the present study was to examine the effects of HDE exposure on intestinal homeostasis. The results from the current study show that HDE (12.5%) intranasal instillations over 3 wk increased intestinal permeability, promoted systemic endotoxemia, induced inflammation in the proximal colon, and disrupted E-cadherin expression in the proximal and distal colon. In addition, HDE exposure elevated mRNA expression of *Lyz1* in the proximal colon. Moreover, *Tnfα* mRNA expression was elevated in the proximal colon, but HDE did not increase the expression of other proinflammatory cytokines in the intestine. Collectively, these findings emphasize the extrapulmonary manifestations of agricultural dust inhalation. More specifically, these data highlight the connection between an intranasally administered environmental trigger causing permeability in the gut and elevating the presence of inflammatory biomarkers (e.g., *Tnfα*, serum endotoxins). This is particularly

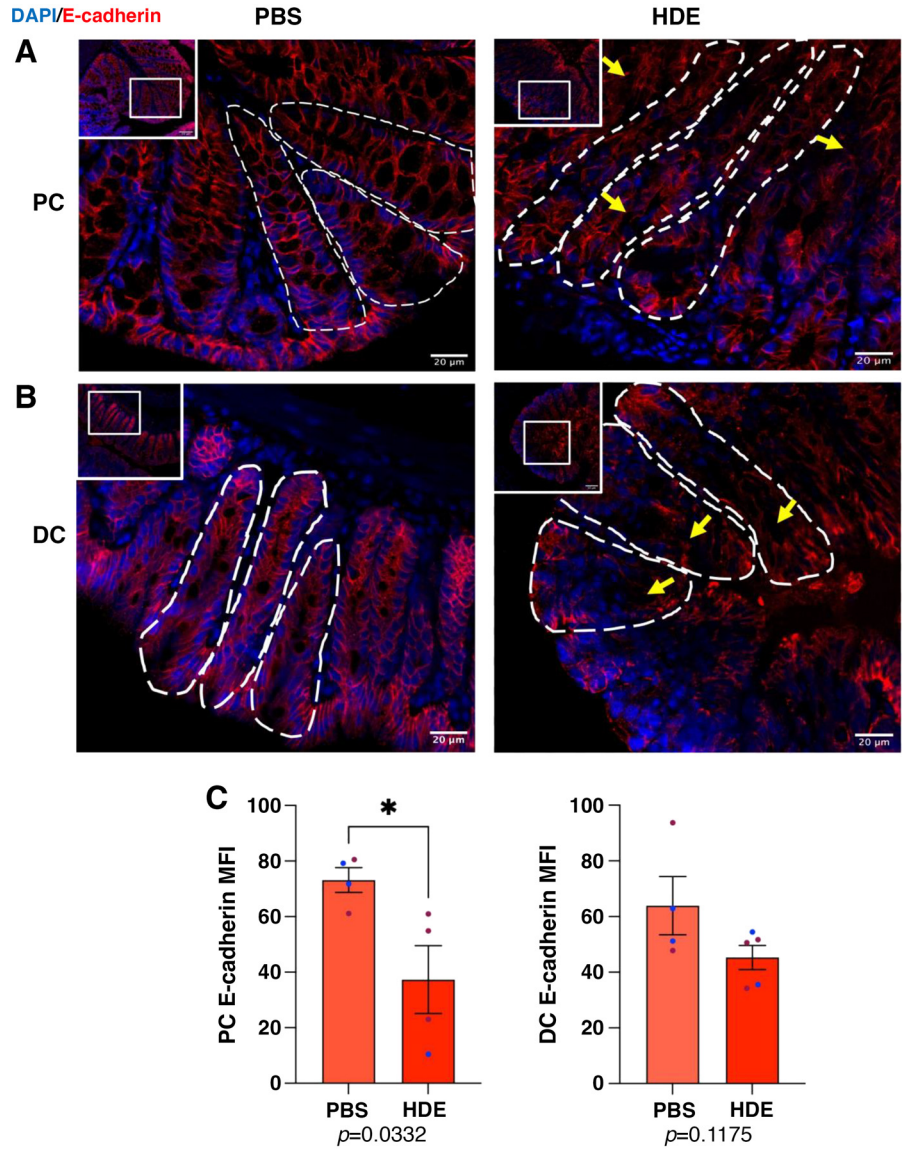

Figure 6. Examination of intestinal epithelial barrier integrity following repetitive HDE exposure. Immunostaining of E-cadherin in colon sections revealed mislocalization and disruption (indicated by yellow arrows) of E-cadherin in the proximal and distal colon of HDE-treated mice (*A* and *B*). Quantification of E-cadherin mean fluorescence intensity (MFI; *C*) showed a significant decrease in the proximal colon (*$P < 0.05$, paired *t* test, $P = 0.0332$, $n = 4$/group) of HDE-treated mice. In addition, the distal colon of HDE-treated mice showed a decreasing trend in E-cadherin fluorescence ($P = 0.1651$, $n = 4$/group). The sex of each mouse is depicted by the data point color [light/pink (female) or light/blue (male)]. DC, distal colon; HDE, hog dust extract; PC, proximal colon.

important for agricultural and CAFO workers who are at greater risk of developing severe respiratory disorders and gastrointestinal diseases (30, 31).

The capability of the airways to respond to agricultural dust and other stimuli has been extensively investigated along with the examination of potential treatments (18). The results of the current study demonstrate that repetitive HDE exposure promotes alveolar inflammation (Fig. 1*A*). This was also corroborated by elevated numbers of infiltrating immune cells (e.g., neutrophils) in the bronchoalveolar lavage fluid of HDE-treated mice (Fig. 2). In addition, HDE exposure increased intestinal permeability as evidenced by elevated serum FD4 and RD70 concentrations, increased intestinal *Tnfα* expression and increased serum LPS. These data indicate involvement of the gut-lung axis as an essential feature in the response to HDE exposure.

Gut injury is characterized by increased intestinal permeability involving the unrestricted pathway coupled with dysregulated intestinal epithelial cell death (32, 33). Particulate matter (PM) air pollution has been shown to compromise intestinal barrier function. PM exposure, intranasally or by oral gavage, has been shown to disrupt tight junctions and increase permeability in colorectal adenocarcinoma (Caco-2) epithelial monolayers in vitro, whereas in vivo studies in mice given 200 mg of PM via gastric gavage, exhibited increased intestinal permeability, elevated IL-6 mRNA expression, and altered localization of zona occludens (ZO)-1 (11). Moreover, colonic sections from mice exposed to PM for 48 h showed increased TUNEL-positive cells (11), thus further marking increased barrier dysfunction. Similarly, our data show a significant increase in TUNEL-positive cells in the small intestine and proximal colon of HDE-treated mice (Supplemental Fig. S1). Although our findings show increased FD4 and RD70 permeability, an increase in TUNEL-positive cells as well as endotoxemia following HDE exposure, there was no further evidence of altered intestinal morphology. Of note, in vitro and in vivo studies suggest that physiologically relevant concentrations of LPS can increase intestinal permeability without inducing epithelial cell death or damage to the intestinal mucosal barrier (25). This is due to an increase in intestinal

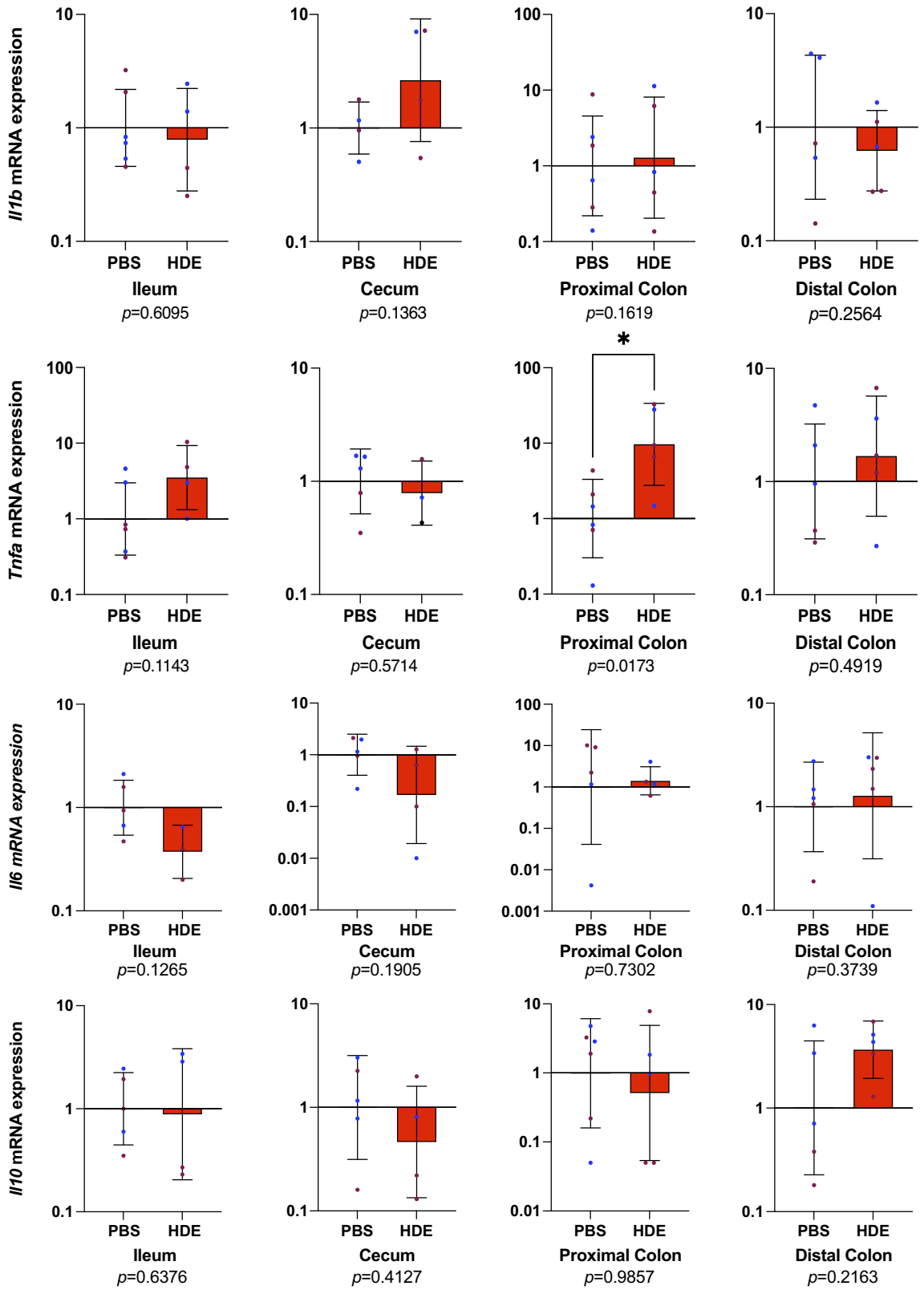

Figure 7. Intestinal epithelial responses initiated by HDE. Inflammatory genes were examined in intestinal whole tissue lysates by qPCR. *Tnfα* expression was increased in the proximal colon (*$P < 0.05$, unpaired *t* test, $P = 0.0173$; $n = 5$–6/group) but not in the ileum, cecum, or distal colon of HDE-treated mice. Conversely, *Il1b* (unpaired *t* test, $P < 0.05$; $n = 3$–4 group), *Il6* (unpaired *t* test, $P < 0.05$; $n = 4$–6/group), and *Il10* (unpaired *t* test, $P < 0.05$; $n = 4$–6/group) were not significantly altered along the intestinal tract. The sex of each mouse is depicted by the data point color [light/pink (female) or light/blue (male)]. HDE, hog dust extract.

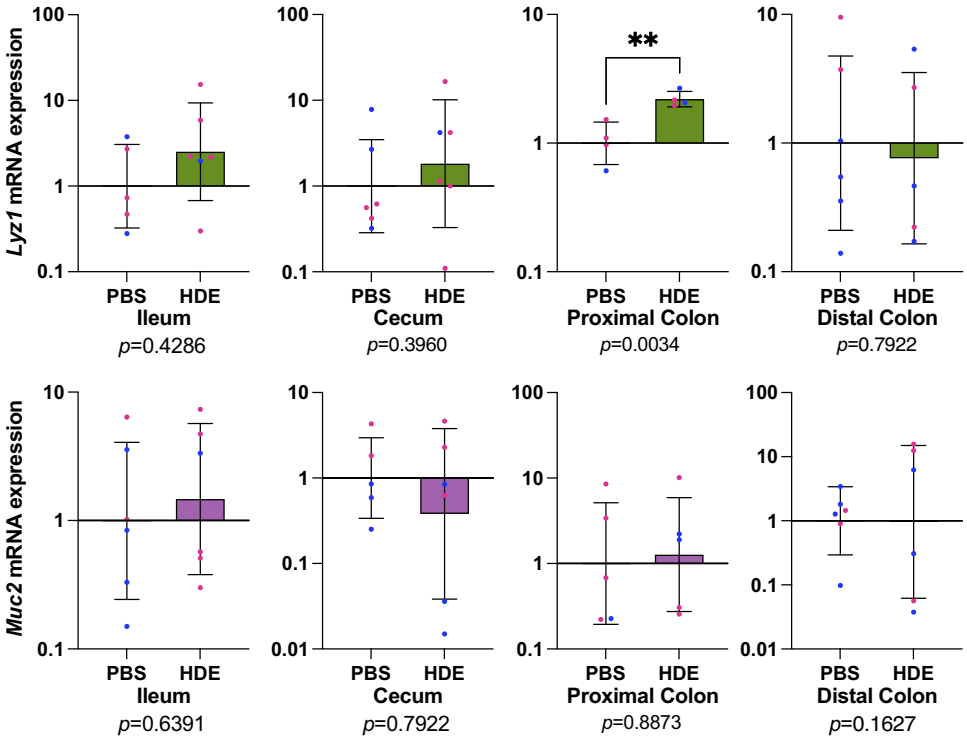

Figure 8. HDE effects on epithelial cell differentiation. After HDE treatment, mRNA expression of the Paneth cell-associated marker *Lyz1* (lysozyme) was unchanged in ileum but was increased in proximal colon epithelial cells (**$P < 0.001$, paired t test, $P = 0.0034$, $n = 4$/group) of HDE-treated mice. Moreover, the expression of goblet cell marker *Muc2* was unaltered in the small and large intestines of HDE-exposed mice. The sex of each mouse is depicted by the data point color [light/pink (female) or light/blue (male)]. HDE, hog dust extract.

epithelial cell expression and membrane localization of toll-like receptor (TLR)-4 (25), emphasizing the role of TLR-4 signal transduction in intestinal barrier regulation. Examination of the LPS/TLR-4 signaling cascade in this study showed a significant increase in TLR-4 protein expression in the proximal colon of HDE-exposed mice (Supplemental Fig. S4). When LPS binds to TLR-4 located on the basolateral membrane of enterocytes (34) this activation of TLR-4 initiates an array of intracellular signaling pathways and a subsequent inflammatory response (34) which is thought to have a role in the progression of inflammatory bowel diseases (IBD).

We also demonstrated that repetitive HDE exposure upregulates *Tnfα mRNA* expression in the proximal colon. Previous studies have reported increases in intestinal *Tnfα* expression following exposure to environmental pollutants (12, 35). In addition, elevated TNF-α exposure of the intestinal epithelium can downregulate cell adhesion molecules and alter intestinal barrier integrity (36, 37). We theorize that LPS found in 12.5% HDE may bind to TLR-4 on intestinal epithelial cells, thereby promoting an increase in *Tnfα* expression.

We further show that repetitive HDE exposure causes intestinal E-cadherin disruption in the proximal and distal colon. E-cadherin is required for tight junction and tissue barrier formation and is the main cadherin expressed in the colonic crypt epithelium (38). Under inflammatory conditions such as IBD, E-cadherin is dysregulated and its loss in intestinal epithelial cells promotes barrier disruption and impairs the localization and function of goblet and Paneth cells (39). Typically, Paneth cells are located in the small intestinal crypts of Lieberkühn and produce antimicrobial proteins, including lysozyme (40). Prior studies suggest that increased expression of lysozyme in the colon is a hallmark of colonic inflammation (41, 42). In our investigation, we found that HDE exposure significantly elevated mRNA expression of *Lyz1* in the proximal colon of mice, further demonstrating evidence of colonic inflammation following agricultural dust exposure. However, HDE-treated mice also exhibited a trend toward elevated mRNA expression of *Muc2* in the distal colon. In rodent models of DSS-induced colitis, the number of goblet cells is significantly reduced in the distal colon but there is an increase in *Muc2* precursor biosynthesis (43). This may imply that individual goblet cells in the distal colon synthesize more *Muc2*, possibly in an attempt to compensate for reduced goblet cell number and offer some residual protection to the colonic epithelium during disease progression (43). In HDE-treated mice, we observed evidence of low-grade inflammation (e.g., endotoxemia), but there were no significant alterations in goblet cell numbers in the colon, reflecting the overall milder histological phenotype compared with active colitis.

Although the respiratory effects of air pollution and agricultural dust have been well characterized, there are a lack of studies investigating the consequences of inhaled agricultural pollutants on intestinal barrier function. We recognize that there are limitations in the current study. This study has yet to identify the primary site of inflammation following HDE exposure. In addition, we did not examine immune cell markers and the response of the remaining secretory cells (e.g., Tuft and enteroendocrine cells) in response to HDE exposure. In the present study, we demonstrated that repetitive exposure to agricultural pollutants from swine farms has a profound impact on gastrointestinal physiology and induces phenotypic differentiation along the intestinal tract. More specifically, our data indicate that agricultural pollutants, including LPS, induce inflammation and alter gene expression of secretory epithelial cells in the proximal colon, and increase intestinal permeability by altering the expression of cell adhesion molecules (e.g., E-cadherin) in the proximal and

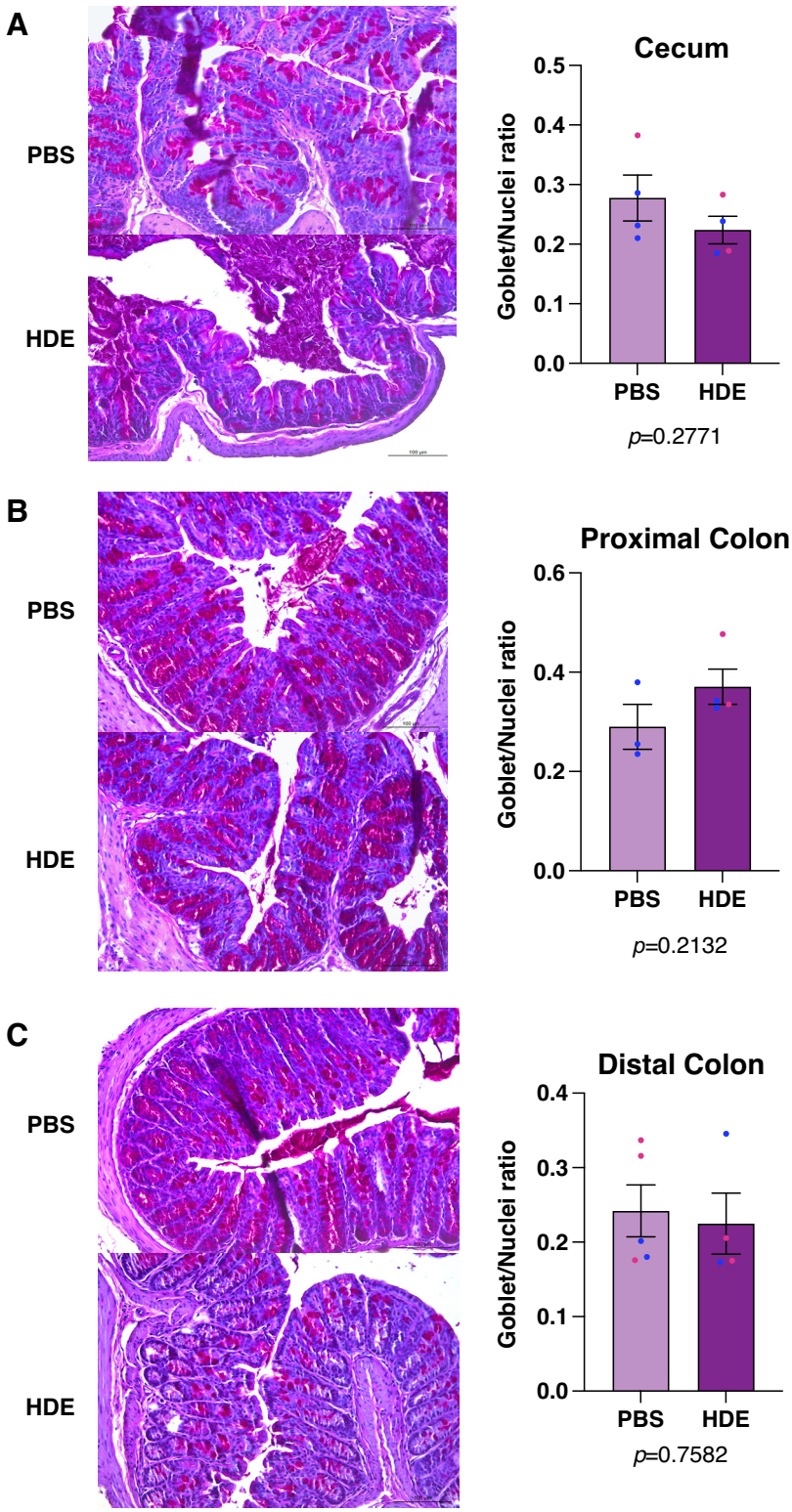

Figure 9. PAS staining of intestinal goblet cells following HDE exposure. Quantification of goblet cells in the cecum (unpaired *t* test, $P = 0.2771$; $n = 4$/group; *A*), proximal (unpaired *t* test, $P = 0.2132$; $n = 3$ or 4/group; *B*), and distal (unpaired *t* test, $P = 7{,}582$; $n = 4$ or 5/group; *C*) colon show no significant differences between HDE-treated mice in comparison with saline controls. The sex of each mouse is depicted by the data point color [light/pink (female) or light/blue (male)]. HDE, hog dust extract; PAS, Periodic Acid-Schiff.

distal colon. Agricultural workers are regularly exposed to CAFO dusts, and in addition to pulmonary consequences, it is unclear if the exposure affects intestinal barrier function. Therefore, ongoing investigation of the physiological consequences of inhaled agricultural dusts is important for the prevention of mucosal diseases and the development of treatments and interventions to limit the consequences of workplace environmental exposures.

DATA AVAILABILITY

Data will be made available upon reasonable request.

SUPPLEMENTAL DATA

Supplemental Fig. S1: 10.6084/m9.figshare.24312418.
Supplemental Fig. S2: 10.6084/m9.figshare.24312421.
Supplemental Fig. S3: 10.6084/m9.figshare.24312424.
Supplemental Fig. S4: 10.6084/m9.figshare.24312427.

ACKNOWLEDGMENTS

The authors thank The University of California, Irvine Experimental Tissue Shared Resource Facility for lung tissue histology processing and Dr. Christopher Weber (University of Chicago, Medicine) for expertise in scoring the intestines for histology and inflammation.

GRANTS

This project was supported by National Institutes of Health Grants 2R01DK091281 (to D.F.M.), 1R01AI153314 (to D.F.M.), 1R01DK130373 (to D.F.M.), R00ES025819 (to T.M.N.), R01HL158926 (to T.M.N.), and by funding from The University of California, Davis-Western Center for Agricultural Health and Safety Grant U54OH007550 (to M.S.C.). M.S.C. was supported by the University of California Presidential Postdoctoral Fellowship Program. B.R.M. was supported by a grant from the National Institutes of Health (T34GM062756).

DISCLOSURES

No conflicts of interest, financial or otherwise, are declared by the authors.

AUTHOR CONTRIBUTIONS

T.M.N. and D.F.M. conceived and designed research; M.S.C., A.U., B.M.R., A.N.S., P.C., V.C., S.M., and H.L. performed experiments; M.S.C., A.U., B.M.R., and T.M.N. analyzed data; M.S.C., A.U., T.M.N., and D.F.M. interpreted results of experiments; M.S.C. prepared figures; M.S.C. drafted manuscript; M.S.C., A.U., T.M.N., and D.F.M. edited and revised manuscript; M.S.C., A.U., T.M.N., and D.F.M. approved final version of manuscript.

REFERENCES

1. **Domingo N**, **Balasubramanian S**, **Thakrar SK**, **Clark MA**, **Adams PJ**, **Marshall JD**, **Muller NZ**, **Pandis SN**, **Polasky S**, **Robinson AL**, **Tessum CW**, **Tilman D**, **Tschofen P**, **Hill JD.** Air quality-related health damages of food. *Proc Natl Acad Sci USA* 118: e2013637118, 2021. doi:10.1073/pnas.2013637118.
2. **Boissy RJ**, **Romberger DJ**, **Roughead WA**, **Weissenburger-Moser L**, **Poole JA**, **LeVan TD.** Shotgun pyrosequencing metagenomic analyses of dusts from swine confinement and grain facilities. *PLoS One* 9: e95578, 2014. doi:10.1371/journal.pone.0095578.
3. **Brunekreef B**, **Strak M**, **Chen J**, **Andersen ZJ**, **Atkinson R**, **Bauwelinck M**, **et al.** Mortality and morbidity effects of long-term exposure to low-level PM2.5, BC, NO_2, and O_3: an analysis of European cohorts in the ELAPSE project. *Res Rep Health Eff Inst* 2021: 1–127, 2021.
4. **Villeneuve PJ**, **Chen L**, **Stieb D**, **Rowe BH.** Associations between outdoor air pollution and emergency department visits for stroke in Edmonton, Canada. *Eur J Epidemiol* 21: 689–700, 2006. doi:10.1007/s10654-006-9050-9.
5. **Kaplan GG**, **Szyszkowicz M**, **Fichna J**, **Rowe BH**, **Porada E**, **Vincent R**, **Madsen K**, **Ghosh S**, **Storr M.** Non-specific abdominal pain and air pollution: a novel association. *PLoS One* 7: e47669, 2012. doi:10.1371/journal.pone.0047669.
6. **Nordgren TM**, **Bailey KL.** Pulmonary health effects of agriculture. *Curr Opin Pulm Med* 22: 144–149, 2016. doi:10.1097/MCP.0000000000000247.
7. **Romberger DJ**, **Bodlak V**, **Von Essen SG**, **Mathisen T**, **Wyatt TA.** Hog barn dust extract stimulates IL-8 and IL-6 release in human bronchial epithelial cells via PKC activation. *J Appl Physiol (1985)* 93: 289–296, 2002. doi:10.1152/japplphysiol.00815.2001.
8. **Poole JA**, **Wyatt TA**, **Oldenburg PJ**, **Elliott MK**, **West WW**, **Sisson JH**, **Von Essen SG**, **Romberger DJ.** Intranasal organic dust exposure-induced airway adaptation response marked by persistent lung inflammation and pathology in mice. *Am J Physiol Lung Cell Mol Physiol* 296: L1085–L1095, 2009. doi:10.1152/ajplung.90622.2008.
9. **Nordgren TM**, **Bauer CD**, **Heires AJ**, **Poole JA**, **Wyatt TA**, **West WW**, **Romberger DJ.** Maresin-1 reduces airway inflammation associated with acute and repetitive exposures to organic dust. *Transl Res* 166: 57–69, 2015. doi:10.1016/j.trsl.2015.01.001.
10. **Johnson AN**, **Harkema JR**, **Nelson AJ**, **Dickinson JD**, **Kalil J**, **Duryee MJ**, **Thiele GM**, **Kumar B**, **Singh AB**, **Gaurav R**, **Glover SC**, **Tang Y**, **Romberger DJ**, **Kielian T**, **Poole JA.** MyD88 regulates a prolonged adaptation response to environmental dust exposure-induced lung disease. *Respir Res* 21: 97, 2020. doi:10.1186/s12931-020-01362-8.
11. **Mutlu EA**, **Engen PA**, **Soberanes S**, **Urich D**, **Forsyth CB**, **Nigdelioglu R**, **Chiarella SE**, **Radigan KA**, **Gonzalez A**, **Jakate S**, **Keshavarzian A**, **Budinger GR**, **Mutlu GM.** Particulate matter air pollution causes oxidant-mediated increase in gut permeability in mice. *Part Fibre Toxicol* 8: 19, 2011. doi:10.1186/1743-8977-8-19.
12. **Kish L**, **Hotte N**, **Kaplan GG**, **Vincent R**, **Tso R**, **Gänzle M**, **Rioux KP**, **Thiesen A**, **Barkema HW**, **Wine E**, **Madsen KL.** Environmental particulate matter induces murine intestinal inflammatory responses and alters the gut microbiome. *PLoS One* 8: e62220, 2013. doi:10.1371/journal.pone.0062220.
13. **Radon K**, **Danuser B**, **Iversen M**, **Jörres R**, **Monso E**, **Opravil U**, **Weber C**, **Donham KJ**, **Nowak D.** Respiratory symptoms in European animal farmers. *Eur Respir J* 17: 747–754, 2001. doi:10.1183/09031936.01.17407470.
14. **Iversen M**, **Kirychuk S**, **Drost H**, **Jacobson L.** Human health effects of dust exposure in animal confinement buildings. *J Agric Saf Health* 6: 283–288, 2000. doi:10.13031/2013.1911.
15. **May JJ**, **Stallones L**, **Darrow D**, **Pratt DS.** Organic dust toxicity (pulmonary mycotoxicosis) associated with silo unloading. *Thorax* 41: 919–923, 1986. doi:10.1136/thx.41.12.919.
16. **Von Essen S**, **Romberger D.** The respiratory inflammatory response to the swine confinement building environment: the adaptation to respiratory exposures in the chronically exposed worker. *J Agric Saf Health* 9: 185–196, 2003. doi:10.13031/2013.13684.
17. **Von Essen SG**, **Thompson AB**, **Robbins RA**, **Jones KK**, **Dobry CA**, **Rennard SI.** Lower respiratory tract inflammation in grain farmers. *Am J Ind Med* 17: 75–76, 1990. doi:10.1002/ajim.4700170119.
18. **Ulu A**, **Sveiven S**, **Bilg A**, **Velazquez JV**, **Diaz M**, **Mukherjee M**, **Yuil-Valdes AG**, **Kota S**, **Burr A**, **Najera A**, **Nordgren TM.** IL-22 regulates inflammatory responses to agricultural dust-induced airway inflammation. *Toxicol Appl Pharmacol* 446: 116044, 2022. doi:10.1016/j.taap.2022.116044.
19. **Wyatt TA**, **Nemecek M**, **Chandra D**, **DeVasure JM**, **Nelson AJ**, **Romberger DJ**, **Poole JA.** Organic dust-induced lung injury and repair: Bi-directional regulation by TNFα and IL-10. *J Immunotoxicol* 17: 153–162, 2020. doi:10.1080/1547691X.2020.1776428.
20. **Ulu A**, **Burr A**, **Heires AJ**, **Pavlik J**, **Larsen T**, **Perez PA**, **Bravo C**, **DiPatrizio NV**, **Baack M**, **Romberger DJ**, **Nordgren TM.** A high docosahexaenoic acid diet alters lung inflammation and recovery following repetitive exposure to aqueous organic dust extracts. *J Nutr Biochem* 97: 108797, 2021. doi:10.1016/j.jnutbio.2021.108797.
21. **Nordgren TM**, **Heires AJ**, **Bailey KL**, **Katafiasz DM**, **Toews ML**, **Wichman CS**, **Romberger DJ.** Docosahexaenoic acid enhances amphiregulin-mediated bronchial epithelial cell repair processes following organic dust exposure. *Am J Physiol Lung Cell Mol Physiol* 314: L421–L431, 2018. doi:10.1152/ajplung.00273.2017.
22. **Tsai PY**, **Zhang B**, **He WQ**, **Zha JM**, **Odenwald MA**, **Singh G**, **Tamura A**, **Shen L**, **Sailer A**, **Yeruva S**, **Kuo WT**, **Fu YX**, **Tsukita S**, **Turner JR.** IL-22 upregulates epithelial claudin-2 to drive diarrhea and enteric pathogen clearance. *Cell Host Microbe* 21: 671–681.e4, 2017. doi:10.1016/j.chom.2017.05.009.
23. **Marchelletta RR**, **Krishnan M**, **Spalinger MR**, **Placone TW**, **Alvarez R**, **Sayoc-Becerra A**, **Canale V**, **Shawki A**, **Park YS**, **Bernts LH**, **Myers S**, **Tremblay ML**, **Barrett KE**, **Krystofiak E**, **Kachar B**, **McGovern DP**, **Weber CR**, **Hanson EM**, **Eckmann L**, **McCole DF.** T

cell protein tyrosine phosphatase protects intestinal barrier function by restricting epithelial tight junction remodeling. *J Clin Invest* 131: e138230, 2021. doi:10.1172/JCI138230.

24. **Kwon J**, **Lee C**, **Heo S**, **Kim B**, **Hyun C-K.** DSS-induced colitis is associated with adipose tissue dysfunction and disrupted hepatic lipid metabolism leading to hepatosteatosis and dyslipidemia in mice. *Sci Rep* 11: 5283, 2021. doi:10.1038/s41598-021-84761-1.
25. **Guo S**, **Al-Sadi R**, **Said HM**, **Ma TY.** Lipopolysaccharide causes an increase in intestinal tight junction permeability in vitro and in vivo by inducing enterocyte membrane expression and localization of TLR-4 and CD14. *Am J Pathol* 182: 375–387, 2013. doi:10.1016/j.ajpath.2012.10.014.
26. **Zhang Z**, **Zhu D**, **Cui B**, **Ding R**, **Shi X**, **He P.** Association between particulate matter air pollution and lung cancer. *Thorax* 75: 85–87, 2020. doi:10.1136/thoraxjnl-2019-213722.
27. **Gao N**, **Xu W**, **Ji J**, **Yang Y**, **Wang ST**, **Wang J**, **Chen X**, **Meng S**, **Tian X**, **Xu KF.** Lung function and systemic inflammation associated with short-term air pollution exposure in chronic obstructive pulmonary disease patients in Beijing, China. *Environ Health* 19: 12, 2020. doi:10.1186/s12940-020-0568-1.
28. **Park J**, **Kim HJ**, **Lee CH**, **Lee CH**, **Lee HW.** Impact of long-term exposure to ambient air pollution on the incidence of chronic obstructive pulmonary disease: a systematic review and meta-analysis. *Environ Res* 194: 110703, 2021. doi:10.1016/j.envres.2020.110703.
29. **Kaplan GG**, **Hubbard J**, **Korzenik J**, **Sands BE**, **Panaccione R**, **Ghosh S**, **Wheeler AJ**, **Villeneuve PJ.** The inflammatory bowel diseases and ambient air pollution: a novel association. *Am J Gastroenterol* 105: 2412–2419, 2010. doi:10.1038/ajg.2010.252.
30. **Guo Y**, **Ryan U**, **Feng Y**, **Xiao L.** Association of common zoonotic pathogens with concentrated animal feeding operations. *Front Microbiol* 12: 810142, 2021. doi:10.3389/fmicb.2021.810142.
31. **Quist AJL**, **Holcomb DA**, **Fliss MD**, **Delamater PL**, **Richardson DB**, **Engel LS.** Exposure to industrial hog operations and gastrointestinal illness in North Carolina, USA. *Sci Total Environ* 830: 154823, 2022. doi:10.1016/j.scitotenv.2022.154823.
32. **Subramanian S**, **Geng H**, **Tan XD.** Cell death of intestinal epithelial cells in intestinal diseases. *Sheng Li Xue Bao* 72: 308–324, 2020.
33. **Chanez-Paredes SD**, **Abtahi S**, **Kuo WT**, **Turner JR.** Differentiating between tight junction-dependent and tight junction-independent intestinal barrier loss in vivo. *Methods Mol Biol* 2367: 249–271, 2021. doi:10.1007/7651_2021_389.
34. **Nighot M**, **Al-Sadi R**, **Guo S**, **Rawat M**, **Nighot P**, **Watterson MD**, **Ma TY.** Lipopolysaccharide-induced increase in intestinal epithelial tight permeability is mediated by toll-like receptor 4/myeloid differentiation primary response 88 (MyD88) activation of myosin light chain kinase expression. *Am J Pathol* 187: 2698–2710, 2017. doi:10.1016/j.ajpath.2017.08.005.
35. **Fitch MN**, **Phillippi D**, **Zhang Y**, **Lucero J**, **Pandey RS**, **Liu J**, **Brower J**, **Allen MS**, **Campen MJ**, **McDonald JD**, **Lund AK.** Effects of inhaled air pollution on markers of integrity, inflammation, and microbiota profiles of the intestines in Apolipoprotein E knockout mice. *Environ Res* 181: 108913, 2020. doi:10.1016/j.envres.2019.108913.
36. **Su L**, **Nalle SC**, **Shen L**, **Turner ES**, **Singh G**, **Breskin LA**, **Khramtsova EA**, **Khramtsova G**, **Tsai PY**, **Fu YX**, **Abraham C**, **Turner JR.** TNFR2 activates MLCK-dependent tight junction dysregulation to cause apoptosis-mediated barrier loss and experimental colitis. *Gastroenterology* 145: 407–415, 2013. doi:10.1053/j.gastro.2013.04.011.
37. **Leppkes M**, **Roulis M**, **Neurath MF**, **Kollias G**, **Becker C.** Pleiotropic functions of TNF-α in the regulation of the intestinal epithelial response to inflammation. *Int Immunol* 26: 509–515, 2014. doi:10.1093/intimm/dxu051.
38. **Daulagala AC**, **Bridges MC**, **Kourtidis A.** E-cadherin beyond structure: a signaling hub in colon homeostasis and disease. *Int J Mol Sci* 20: 2756, 2019. doi:10.3390/ijms20112756.
39. **Grill JI**, **Neumann J**, **Hiltwein F**, **Kolligs FT**, **Schneider MR.** Intestinal E-cadherin deficiency aggravates dextran sodium sulfate-induced colitis. *Dig Dis Sci* 60: 895–902, 2015. doi:10.1007/s10620-015-3551-x.
40. **Lueschow SR**, **McElroy SJ.** The Paneth cell: the curator and defender of the immature small intestine. *Front Immunol* 11: 587, 2020. doi:10.3389/fimmu.2020.00587.
41. **Simmonds N**, **Furman M**, **Karanika E**, **Phillips A**, **Bates AW.** Paneth cell metaplasia in newly diagnosed inflammatory bowel disease in children. *BMC Gastroenterol* 14: 93, 2014. doi:10.1186/1471-230X-14-93.
42. **Yu S**, **Balasubramanian I**, **Laubitz D**, **Tong K**, **Bandyopadhyay S**, **Lin X**, **Flores J**, **Singh R**, **Liu Y**, **Macazana C**, **Zhao Y**, **Béguet-Crespel F**, **Patil K**, **Midura-Kiela MT**, **Wang D**, **Yap GS**, **Ferraris RP**, **Wei Z**, **Bonder EM**, **Häggblom MM**, **Zhang L**, **Douard V**, **Verzi MP**, **Cadwell K**, **Kiela PR**, **Gao N.** Paneth cell-derived lysozyme defines the composition of mucolytic microbiota and the inflammatory tone of the intestine. *Immunity* 53: 398–416.e8, 2020. doi:10.1016/j.immuni.2020.07.010.
43. **Renes IB**, **Boshuizen JA**, **Van Nispen DJ**, **Bulsing NP**, **Büller HA**, **Dekker J**, **Einerhand AW.** Alterations in Muc2 biosynthesis and secretion during dextran sulfate sodium-induced colitis. *Am J Physiol Gastrointest Liver Physiol* 282: G382–G389, 2002. doi:10.1152/ajpgi.00229.2001.